Leafiness-LiDAR index and NDVI for identification of temporal patterns in super-intensive almond orchards as response to different management strategies

L. Sandonís-Pozo, Baptiste Oger, Bruno Tisseyre, J. Llorens, A. Escolà, M. Pascual, J.A. Martínez-Casasnovas

European Journal of Agronomy 159 (2024) 127278

Contents lists available at ScienceDirect

European Journal of Agronomy

journal homepage: www.elsevier.com/locate/eja

Leafiness-LiDAR index and NDVI for identification of temporal patterns in super-intensive almond orchards as response to different management strategies

L. Sandonís-Pozo [a,*], B. Oger [b], B. Tisseyre [b], J. Llorens [a,c], A. Escolà [a], M. Pascual [d], J.A. Martínez-Casasnovas [a]

[a] Research Group in AgroICT Precision Agriculture (GRAP), Universitat de Lleida-Agrotecnio CERCA Center, Av. Alcalde Rovira Roure, 191, Catalonia E25198, Spain
[b] ITAP, Univ. Montpellier, INRAE, Institut Agro, 2 Place Pierre Viala, Montpellier 34060, France
[c] Serra Húnter Fellowship, Universitat de Lleida, Av. Alcalde Rovira Roure, 191, Catalonia E25198, Spain
[d] Department of Horticulture, Botany and Gardening, Universitat de Lleida, Av. Alcalde Rovira Roure, 191, Catalonia E25198, Spain

ARTICLE INFO

Keywords:
Perennial crop
Summer pruning
Canopy monitoring
Orchard management
LAI
Leafiness-LiDAR index
Sentinel-2
NDVI time series
ECa
Google Earth Engine (GEE)
Spearman's rank correlation
S2cloudless
Model-based clustering
Mclust
Potential management zones (PMZs)
Precision horticulture

ABSTRACT

The use of super-intensive orchards is a growing trend in fruit production. The present study aims to improve management of these cropping systems by focusing on how agronomic decisions impact orchard dynamics in the short to medium term and by providing a decision-support approach based on stable temporal patterns from previous seasons. A multitemporal study using remote sensing and LiDAR was conducted in a commercial almond orchard over four growing seasons (2019–2022) to determine the optimal timing of image acquisition for variable pre-harvest treatments. A model-based clustering (*mclust*) was applied to optimal Sentinel-2 NDVI maps and apparent soil electrical conductivity (ECa) data, interpolated to the pixel centroids of Sentinel-2 image grids, to delineate potential management zones (PMZs). The leafiness-LiDAR index (LLI), a leaf area index (LAI) estimator, was obtained as ground truth after summer pruning and before harvesting, showing a significant influence of fertigation and pruning on the LAI, with summer pruning particularly influencing orchard dynamics. The optimal time for NDVI mapping was found to be two months after summer pruning in productive years and two weeks after in unproductive years. The delineated PMZs were consistent across seasons and corresponded to significant LAI differences. This method could contribute to improving resource management and sustainability in super-intensive commercial orchards.

1. Introduction

The global fruit industry is moving towards new, more efficient and profitable high-density cropping systems (Maldera et al., 2021). Super-intensive systems, with over 1500–2500 trees ha^{-1} or more, offer economic advantages such as increased mechanisation, improved harvesting efficiency and early production compared to traditional rainfed orchards (Arquero and Jarvis-Shean., 2017). For this reason, the almond sector in Mediterranean countries has undergone a significant transformation in the last decade, displacing other crops with lower profitability (Casanova-Gascón et al., 2019). In Spain alone, irrigated almond orchards almost tripled between 2015 and 2020, from 52,990 ha in 2015–139,399 ha in 2020, with exponential growth expected in the coming years (Mirás-Avalos et al., 2023).

However, super-intensive systems present challenges such as planting and management costs, higher susceptibility to diseases and pests, and a potentially shorter orchard life (Arquero and Jarvis-Shean., 2017). In addition, almond trees are highly sensitive to temperature variations (Rodríguez et al., 2018). The increased frequency of extreme climatic events in the Mediterranean region in recent years, such as hail or frost during late winter and early spring (Serrano-Notivoli et al., 2022), can cause significant damage, leading to the loss of buds, flowers, nuts and, consequently, yield (Rodríguez et al., 2018). Given the recent emergence of these cropping systems, growers face uncertainties because of a number of unexplored factors. This poses a challenge to the economic sustainability of orchards, requiring adaptive management

* Corresponding author.
E-mail address: leire.sandonis@udl.cat (L. Sandonís-Pozo).

https://doi.org/10.1016/j.eja.2024.127278
Received 19 April 2024; Received in revised form 8 July 2024; Accepted 8 July 2024
Available online 13 July 2024

strategies and a better understanding of the impact of agronomic decisions in the short and medium term (Casanova-Gascón et al., 2019).

To address these uncertainties, canopy monitoring of super-intensive orchards is becoming increasingly important to ensure consistent quality and meet short- and medium-term production and sustainability targets (Arquero, Jarvis-Shean., 2017). The scientific literature has demonstrated the suitability of emerging technologies that rely heavily on sensors for orchard canopy monitoring (Zude-Sasse et al., 2021). Remote sensing, complementing ground-based sensors, has been widely used to monitor crop growth and estimate quality and yield from local to global scales (Sun et al., 2017; Barajas et al., 2020; Kasimati et al., 2021). High-resolution imagery acquired by unmanned aerial vehicles (UAVs) has proven effective in estimating biophysical and geometric parameters (Johansen et al., 2018; Torres-Sánchez et al., 2018; Caruso et al., 2019). LiDAR (Light Detection and Ranging) technology, particularly mobile terrestrial laser scanning (MTLS), has been used for diverse applications ranging from estimating the leaf area index (LAI, leaf area per unit ground area) to precision spraying and pruning (Zhang et al., 2020; Gu et al., 2021; Mahmud et al., 2021).

However, most studies have focused on full canopy development stages rather than continuous canopy monitoring during and between seasons, which may be more appropriate to adapt management tasks to crop dynamics and characterise spatiotemporal variability in orchards (Vélez et al., 2022). The continuous estimation of LAI is crucial for super-intensive systems (Westling et al., 2021), and authors such as Fang et al. (2019) have highlighted the increasing demand for LAI validation studies and the need for continuous seasonal LAI measurements and time series validation. Traditionally, photosynthetically active radiation (PAR) measurements using ceptometers have been used in horticulture to estimate LAI. However, ceptometer-based measurements require direct sunlight and have limitations in diffuse light conditions (Pokovai and Fodor, 2019). For this reason, it is difficult to obtain PAR measurements in a continuous way, which compromises their use in a precision horticulture context.

Novel studies for continuous LAI estimation in orchards have emerged in recent years. These include the study by Gu et al. (2022), who used an MTLS to scan the canopy of an apple orchard and developed a leaf area detection model, achieving a prediction accuracy of 73.6 % compared to manual measurements of canopy leaf area. A new index for LAI estimation has also recently been introduced by Sandonís-Pozo et al. (2023) called the leafiness-LiDAR index (LLI), which combines LiDAR-derived 3D point cloud parameters such as tree row cross-section and canopy leafiness and can be used for multi-temporal monitoring of orchard canopies. In almonds, LAI information is also useful to avoid imbalances between leaf and fruit N pools, especially at the beginning of production, a period when canopy vegetation can reach very high growth rates (Zarate-Valdez et al., 2015). Previous research has shown that the LAI has strong correlations with satellite-based vegetation indices such as the normalized difference vegetation index (NDVI), which serves as a comprehensive data source summarising the effects of environmental factors and management practices on the canopy (Johnson et al., 2003; Zarate-Valdez et al., 2012; Sun et al., 2017).

In recent years, the emergence of satellite missions such as Sentinel-2, which provide free imagery characterised by high spatial, temporal and spectral resolution, and of platforms such as Google Earth Engine for the processing of large image time series has encouraged the development of a large number of scientific studies on crop dynamics, spatiotemporal monitoring and responses to irrigation and soil management practices (Calera et al., 2017; Bellvert et al., 2021; González-Gómez et al., 2022). The use of time series of NDVI maps together with other data sources such as soil surveys, agronomic management information, yield maps, topography and apparent soil electrical conductivity (ECa) has been highlighted in the scientific literature as a requirement for identifying stable crop patterns and defining management zones in precision agriculture (Vélez et al., 2022; Ouazaa et al., 2022).

In the precision agriculture literature, unsupervised clustering techniques such as fuzzy c-means and k-means have been widely used for mapping management zones for yield prediction and variable rate irrigation (Martínez-Casasnovas et al., 2018; Serrano et al., 2020). However, the increasing heterogeneity and volume of data in precision agriculture is a challenge for these methods, especially when dealing with high-density data files with multiple variables (Saifuzzaman et al., 2019). Research on finite Gaussian mixture models (GMMs) has shown promise for clustering multivariate continuous data in remote sensing image classification (Lagrange et al., 2017; Guan et al., 2023) as well as for automated management zone delineation for fertiliser optimization, yield prediction, and plant oil quality assessment (Lim et al., 2020; Jiwei et al., 2021).

Despite the potential of these models for delineating PMZs, research on their application in super-intensive systems is limited. In perennial crops such as almonds, the identification of stable management zones over multiple seasons could provide valuable information as a decision-support tool for managing operations based on previous seasons. This study aims to fill this gap by investigating the impact of management practices on orchard dynamics and identifying temporal patterns using a model clustering approach to define stable PMZs. In addition, the study aims to determine the optimal timing of image acquisition for the planning of different management actions in the orchard. This timing is crucial from a practical point of view as it allows the maximum time before harvest for image analysis and for making and implementing management decisions. The study also aims to improve the understanding of the relationship over time between the NDVI and other well-understood parameters such as the LAI.

The methodology developed in this research is compatible with commercial orchard conditions and could lead to more effective resource management and improved sustainability in super-intensive almond orchards.

2. Material and methods

2.1. Study area

The study was carried out in a commercial super-intensive almond orchard Prunus dulcis (Mill.) d.A. Webb, cv Lauranne®, located in Raimat (Catalonia, NE Spain, X = 288260 m, Y = 4616100 m, Z = 282 m UTM 31 T/ETRS89). The experiment covered an area of approximately 0.75 ha and 24 tree rows. These 24 rows were selected to avoid the border effect. The orchard was established during the 2016/17 winter with a plantation pattern of 3.2 m x 1.5 m (2083 trees ha^{-1}). The climate is Mediterranean with continental characteristics, strong seasonal temperature variations and an annual rainfall frequently below 400 mm. Meteorological data was collected from an automatic station located 1.8 km from the orchard (X = 287654.66 m, Y = 4617757.24 m, Z = 286.4 m UTM 31 T/ETRS89). The soil type was classified as a Petrocalcic Calcixerept (Soil Survey Staff, 2014). This type of soil is characterized by the presence of a petrocalcic horizon at variable depths that contains high concentrations of calcium carbonate ($CaCO_3$). The depth of this horizon ranges from 50 cm to 80 cm. The soil exhibited good drainage and was not affected by salinity.

2.2. Management tasks in the orchard

The present study comprised four years: 2019, 2020, 2021 and 2022. Table 1 presents the orchard management tasks applied in the orchard during those years and the dates when certain tasks were carried out. The orchard was mechanically pruned with a cutting disk machine in winter to create a hedgerow with a central axis ensuring a fine and low visor branching and also in late spring to early summer to maintain an efficient and active exposed leaf area in order to have the maximum productive potential and to facilitate the work of harvesting machines. The number of pruning interventions was different across the years. 2019 was the first productive year of the plantation and the period in

Table 1
Orchard management tasks and LiDAR surveys in the super-intensive almond orchard along the study years. DOY = Day Of the Year, starting from 1st January. SP = for summer pruning.

Productive seasons						Unproductive seasons					
2019			2020			2021			2022		
Date	DOY	Management task	Date	DOY	Management task	Date	DOY	Management task	Date	DOY	Management task
09/02/2019	40	1st pruning	13/02/2020	44	1st pruning	10/02/2021	41	Weeding	11/02/2022	42	1st pruning
06/03/2019	65	2nd pruning	09/04/2020	100	2nd pruning	06/04/2021	96	1st pruning	23/05/2022	143	2nd pruning
02/05/2019	122	3rd pruning	-	-	-	-	-	-	-	-	-
17/06/2019	168	Weeding	05/05/2020	126	Weeding	15/05/2021	135	Weeding	29/06/2022	180	Weeding
19/06/2019	170	SP(4th)	04/06/2020	156	SP (3rd)	07/06/2021	158	SP (2nd)	06/07/2022	187	SP (3rd)
22/06/2019	173	LiDAR	06/06/2020	158	LiDAR	11/06/2021	162	LiDAR	07/07/2022	188	LiDAR
23/07/2019	204	5th pruning	-	-	-						
20/09/2019	263	LiDAR	04/09/2020	248	LiDAR	17/09/2021	260	LiDAR	23/09/2022	266	LiDAR
27/09/2019	270	Yield (2467 kg ha^{-1})	28/09/2020	272	Yield (3019 kg ha^{-1})	-	-	-	-	-	-
09/12/2019	343	Winter pruning (6th)	03/12/2020	338	Winter pruning (4th)	09/11/2021	313	Winter pruning (3rd)	-	-	-

which more interventions were registered. Inter-row weeds were removed every season before the summer pruning through strimmer passes. Table 1 shows that 2021 and 2022 were unproductive seasons as they were affected by bloom-time frost, resulting in a complete loss of yield in both years.

The orchard was drip irrigated receiving a variable volume of water depending on the year (Table 2). The application of nutrients was carried out using 3 electromagnetic injector pumps with an adjustable flow rate between 0.5 L h^{-1} and 9.0 L h^{-1} (Dositec MP, ITC Dosing Pumps, Barcelona, Spain). The dose rates applied in each season are shown in Table 2. Fertilizer was injected in each irrigation cycle, adjusting the injector pumps to the flow rate and proportion necessary to dose the fertilizer according to the requirements of the crop in each season based on foliar and soil analyses, yields obtained in previous years and field observations.

2.3. Methodological approach

Fig. 2 shows a summary of the methodological approach which is described in detail in the following sections. LiDAR data and Sentinel-2 NDVI time series were acquired and analyzed over four consecutive seasons (2019–2022). Subsequently, the leafiness-LiDAR index (LLI), an estimator of the LAI obtained from LiDAR 3D point clouds was computed and interpolated after summer pruning and before harvest each season. Apparent soil electrical conductivity (ECa), a proxy for soil variability, was also considered as a data source.

To identify the optimal NDVI date(s) for managing pre-harvest crop treatments, a series of Spearman's rank correlation coefficients (r_s), which measure the strength and direction of association between two maps, were calculated between each NDVI and the final LLI maps. The delineation of PMZs was performed using a model-based clustering approach. The clustering model combined the first Sentinel-2 NDVI maps identified within a stable threshold ($Tr_s = 0.60$) together with the ECa to find common vegetation distribution patterns and guide management practices in subsequent years. The variables used in the model are represented in yellow in the flow chart (Fig. 2). The PMZs were validated with the LLI values measured a few days before harvest for each year using an ANOVA post hoc test (p-value ≤ 0.01). This validation process is represented in green in Fig. 2.

2.4. Data sources

2.4.1. LiDAR data acquisition, point cloud generation and data extraction

A total of 24 tree rows (84 m long) were scanned during four seasons using an MTLS equipped with VLP-16 LiDAR sensors (Velodyne Lidar Inc., Silicon Valley, USA), but using different platforms. For the first season, the VLP-16 sensor was mounted on a self-propelled mobile platform at a constant speed of 2 km h^{-1}. The 3D point clouds were georeferenced using a Leica GPS 1200 GNSS-RTK system (Leica, Wetzlar, Germany) (Fig. 3, left). For the following seasons, 2020, 2021 and 2022, the MTLS was a commercial bMS^{3}D–^{4}CAM backpack system (Viametris, Louverné, France), which incorporates two LiDAR VLP-16 sensors (Velodyne, San Jose, CA, USA), a multi-constellation GNSS receiver, an inertial measurement unit and 4 RGB cameras. This MTLS was transported by a person traveling on an electric all-terrain vehicle (eATV) with a scanning speed of about 10 km h^{-1} (Fig. 3, right).

The scans were performed at two important stages for orchard management: after summer pruning (June) and before harvesting (September) (Table 1). Subsequently, eight 3D point clouds of the plot were created and processed by means of self-developed algorithms

Table 2
Nutrient (NPK) inputs and mean temperature (T), accumulated precipitation and evapotranspiration (Eto) during the mid-season period (15th February to 30th September).

Year	Mean T (°C)	Precipitation (mm)	Eto (mm)	Irrigation (m^3 ha^{-1})	N (kg ha^{-1})	P (kg ha^{-1})	K (kg ha^{-1})
2019	17.8	165.4	940.5	427	104.8	47.0	168.0
2020	18.2	271.7	900.7	462	178.0	35.5	266.0
2021	17.7	203.6	879.5	448	127.9	32.7	96.5
2022	19.0	206.5	928.6	435	101.0	34.2	87.3

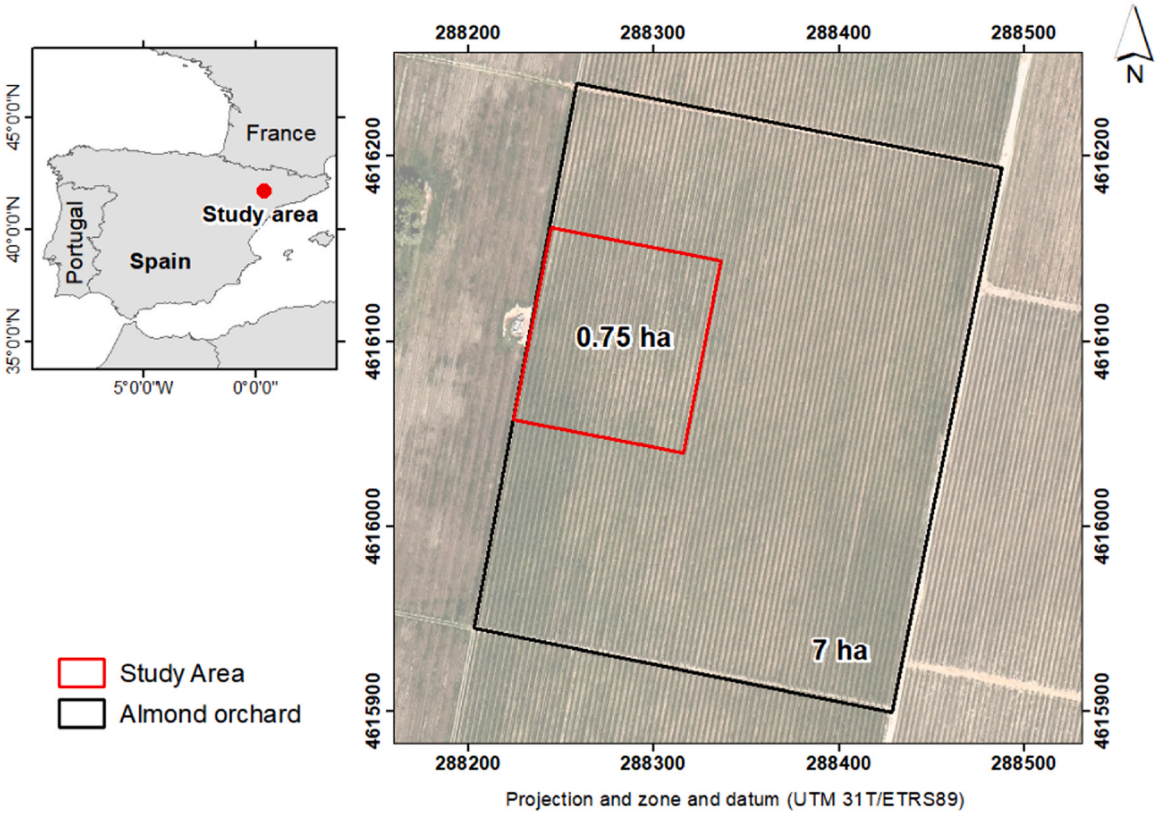

Fig. 1. Location of the study area, almond orchard and tree rows where LiDAR data was acquired.

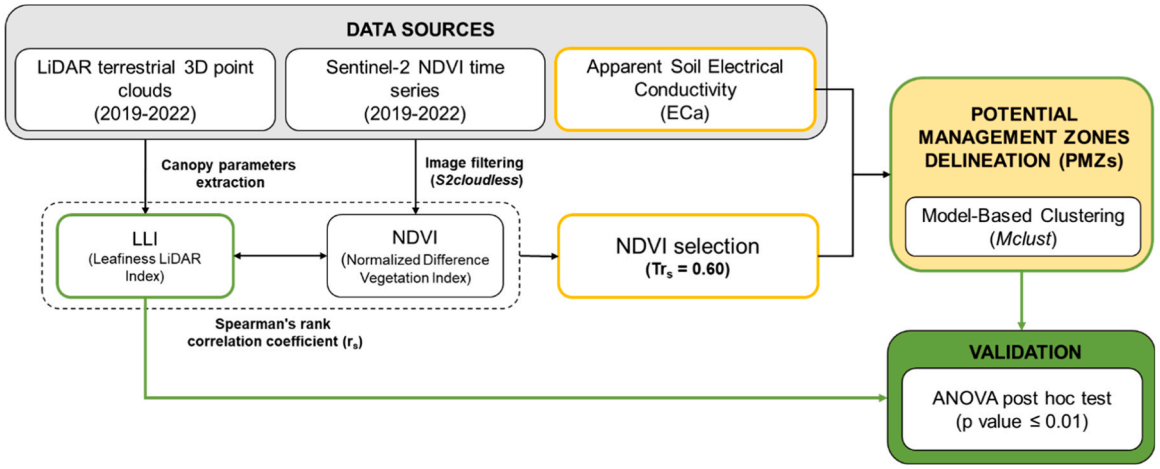

Fig. 2. Flow chart of the methodological approach applied in the present research to identify the optimal NDVI date(s) for managing pre-harvest crop treatments and to delineate potential management zones (PMZs) based on multitemporal data, multispectral imagery and LiDAR data.

described in Llorens et al. (2019). By applying this code, geometric and structural parameters of the canopy were summarized every 0.5 m along each row as described in Sandonís-Pozo et al. (2022).

2.4.2. *Leafiness-LiDAR index (LLI)*

The LLI refers to the ability of the hedgerow to intercept light, being a LAI estimator. The LLI was obtained according to Eq. 1, as the combination of two parameters derived from the LiDAR point clouds processing: a) the cross-section (CS) (m^2), defined as the area occupied by biomass in a plane perpendicular to the longitudinal axis of the row. The CS was calculated by multiplying the maximum width measured each 0.5 m along the orchard rows (ROI-A) and each 0.1 m on the vertical plane (ROI-B); and b) canopy leafiness (L), the opposite of canopy porosity (Porosity-avg), which is related to light penetration. Porosity was calculated as the ratio between the average (left and right scan sides of the row) number of laser beams traversing the canopy with respect to all beams emitted in ROI-A by the LiDAR sensor, expressed as a percentage as described in Sandonis-Pozo et al. (2022).

$$LLI = L * CS \quad (1)$$

where LLI is the leafiness-LiDAR index (m^2), CS is the tree row cross-sectional area (m^2) and L is leafiness (dimensionless).

Fig. 4 offers a graphical representation of the LAI estimation obtained with the LLI index. LLI values were calculated (Eq. 1) every 0.5 m

Fig. 3. MTLS for LiDAR data acquisition: Left: system used in 2019. Right: system used in 2020, 2021 and 2022.

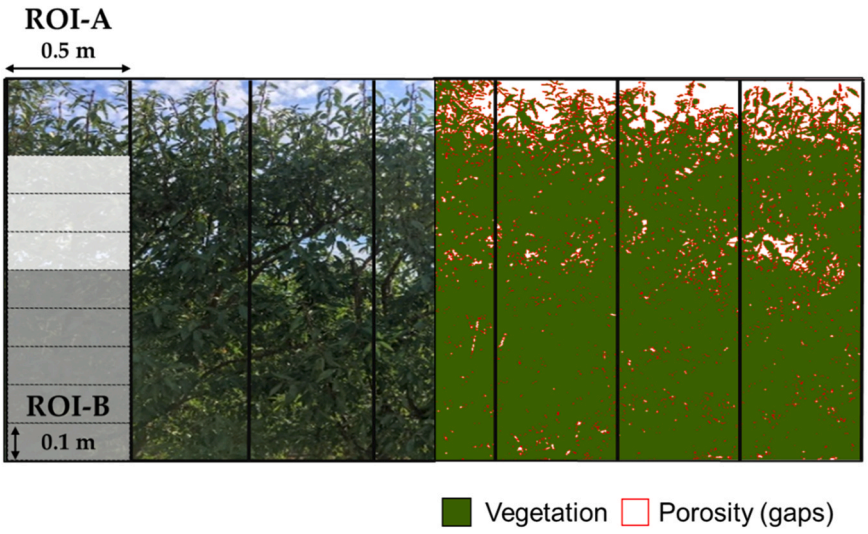

Fig. 4. Graphical representation of the leafiness-LiDAR index. Left: photograph of hedgerow in a super-intensive almond orchard. Right: graphical representation of the LAI estimation obtained with the LLI index. ROI-A and ROI-B represent the different regions of interest used in the process of crop parameter extraction: along the horizontal plane of 0.5 m width along the rows (ROI-A) and along the vertical plane of 0.1 m (ROI-B).

along the tree rows. In total, 4330 sampling points were distributed along the studied rows. These points were then krigged to the centroid Sentinel-2 grid to have the same spatial extent as the Sentinel-2 time series. For this study, only the LLI corresponding to September was mapped using the Precision Agricultural Tool plugin for QGIS 3.16 (Ratcliff et al., 2020), following the methodology described in Sandonís-Pozo et al. (2022).

2.4.3. Time series of remote sensing data

Sentinel-2 L2A images were selected and processed using Google Earth Engine (GEE). The images were used to build a full seasonal time series with a time step of 5 days. From the original Sentinel-2-pixel grid (TILE T31 TBG), a pixel selection was performed to select those containing a similar proportion of vegetation rows. All the multispectral images were clipped to this Sentinel-2 selected grid extension and the NDVI was computed as an average of all the pixels within the Sentinel-2 selected grid boundaries. The period considered for the analysis was from 15th February to 30th September for the four seasons. Images containing clouds or shadows were removed from the database. For this purpose, the *S2cloudless* GEE algorithm was used. The *S2cloudless* is an automated cloud-detection algorithm for Sentinel-2 imagery (Skakun et al., 2022). Clouds were identified from the Sentinel-2 cloud probability dataset (*S2cloudless*) and shadows were defined by cloud projection intersection with low-reflectance near-infrared (NIR) pixels. Finally, for the considered period, 31, 25, 22 and 21 images corresponding to 2019, 2020, 2021 and 2022, were respectively selected and processed.

2.4.4. Soil sampling and apparent electrical conductivity (ECa)

An ECa survey was carried out on 23rd June 2019 with a Dualem 2

sensor (Dualem Inc., Milton, ON, Canada) operated by Agrarium Technologies (Monzón, Spain) and Greenfield Technologies (Badajoz, Spain). The Dualem sensor consists of a dual-geometry array that simultaneously measures both electrical conductivity and magnetic susceptibility to two distinct and defined depths using electromagnetic induction. In the present case, the dual array was configured to work at 0 cm to 30 cm (shallow ECa) and 0 cm to 90 cm (deep ECa) depths. Data was georeferenced using an AgGPS332 GPS receiver (Trimble, Westminster, CO, USA) with EGNOS (European Geostationary Navigation Overlay Service) augmentation to obtain differential global positioning system (DGPS) locations in geographic coordinates WGS84 (EPSG 4326). ECa values were filtered, removing points with values outside the range average ± 2.5 standard deviations according to the criteria of Taylor et al. (2007). The final ECa dataset consisted of 1406 sampling locations with shallow and deep readings. The ECa dataset was krigged to the centroid Sentinel-2 grid to have the same spatial extent as the Sentinel-2 time series following the methodology explained in Section 2.4.2.

A soil texture map was also obtained on 5th July 2019. This texture map was developed after the shallow and deep ECa data acquisition. The ECa values were interpolated by kriging on a 1 m grid and the values were then divided into zones to identify potential areas for sampling. After this variability analysis, a simple soil sampling was carried out in 8 different points within the plot. Samples were collected with the aid of a manual auger hole at two depths (0–30, 30–90) measuring pH, water retention and infiltration rate. The percentages of clay, silt and sand were also determined. Soil was classified as a categorical variable that describes the texture following the USDA classification (Soil Survey Staff, 2014). The predominant soil texture was silt loam and clay loam.

2.5. Data analysis

2.5.1. Intra- and inter-annual leafiness-LiDAR index (LLI) variability

A comparison of the LLI values within and between years was performed using violin plots generated with the Seaborn and Matplotlib libraries in Python 3 (Waskom, 2021). Violin plots enable analysis of the variability of two datasets (Moon, 2016). These graphs combine the information obtained with kernel density plots (KDEs). The wider the plot section, the higher the variability, with the statistical information, such as the mean, median (Q2), and interquartile range (IQR), obtained from box plots. Two groups were considered for each year, with LLI summarizing the points obtained immediately after summer pruning (in June) and those acquired immediately before harvesting (in September).

2.5.2. Sentinel-2 NDVI map selection (inter-annual stability): Spearman rank correlation coefficient

To find the optimal image acquisition date(s) to compute the NDVI to be used as a reference to manage pre-harvest crop treatments, such as N treatments, precision pruning and/or spraying, a rank correlation analysis based on the Spearman rank method was applied between each LLI map computed a few days before harvest and the Sentinel-2 NDVI maps acquired during the mid-season along the four considered years.

In the present study, the Spearman's rank correlation coefficient (r_s) measured the agreement in the correlation of pixels between the NDVI and the LLI pixel maps. This analysis is suitable for data that do not follow a specific distribution and assigns a coefficient to each pair of maps which ranges from −1–1 (Rosenblad, 2011). A Spearman rank correlation coefficient close to ±1 indicates a strong monotonic relationship, while 0 means there is no correlation between the variables. In this case, an arbitrary threshold for the Spearman rank ($Tr_s = 0.6$) was considered to define the date(s) from which the NDVI patterns could be considered stable and similar to that observed at harvest. This threshold value does not correspond to any agronomic indicator, but is considered here as a statistical threshold that corresponds to 80 % of the magnitude of variation of r_s.

2.5.3. Model-based clustering approach to delineate potential management zones (PMZs)

A model-based clustering was applied to find representative distribution patterns over the years and guide management practices by delineating PMZs in the orchard. The model input data were: a) the first Sentinel-2 NDVI map per each year reaching a $Tr_s = 0.6$; b) the shallow ECa; and c) the deep ECa. All were considered important for field variability. The clustering was conducted using the *mclust* package (version 6.0.1.) implemented in Rstudio (Scrucca et al., 2023). This model-based approach is based on finite Gaussian mixture models (GMMs) and uses maximum likelihood to identify the optimal model fit. The best model is selected using the Bayesian information criterion (BIC). A higher BIC value indicates strong evidence in favour of the corresponding model. The contribution of the variables was determined using the *clustvarsel* package, employing a stepwise greedy search algorithm. To validate the delineated PMZs and assist in agronomic decision making, the LLI was used as ground truth. A post-hoc ANOVA test was applied to LLI to determine if this parameter was significantly different in the two delimited PMZs, meaning that differential management of the canopy could be applied to the orchard.

3. Results

3.1. Intra- and inter-year leafiness-LiDAR index (LLI) variability

Fig. 5 shows a series of pictures of the almond orchard in June and September over the years of the experiment. The LLI values for each moment are presented, as well as their intra-annual variation. As explained in the previous section, LLI was considered as an LAI estimator (see 2.4.2). According to these results, the LAI estimated values were higher in September than in June in the first three seasons, with increases of 1.08 m^2, 1.00 m^2 and 0.40 m^2 in 2019, 2020 and 2021, respectively, and a decrease of 0.37 m^2 in 2022.

Fig. 6 presents four violin plots that compare the LLI values within and between years (2019–2022). The plots on the left show the LLI values after summer pruning (June), while those on the right show the values before harvest (September). LLI values were higher for the first two years (2019 and 2020), with 2020 the year in which the highest LLI values were found.

Differences were found when comparing the data distribution patterns across the four years. LLI values were more variable (wider KDE and higher IQR ranges) in 2019 and 2020 than in 2021 and 2022. Regarding intra-annual variability, except for 2022, LLI showed higher variability and higher values at the end of the season, before harvesting.

3.2. Intra- and inter-annual stability of NDVI within-field patterns

Fig. 7 shows the Sentinel-2 NDVI time series computed at plot level as an average of all the pixels within the study area boundaries. The evolution of the Spearman's rank correlation coefficient (r_s) is also presented. The r_s values were calculated between each NDVI pixel value and the corresponding LLI value measured a few days before harvesting in each year. The management practices carried out in the orchard (Table 1) are represented with vertical lines, indicating the day (expressed as DOY) on which a particular operation was completed.

These graphs show that the NDVI was stable over the season. NDVI values before summer pruning ranged from 0.4 to 0.8. However, both NDVI and r_s values changed their trend before and after summer pruning. After summer pruning, NDVI values were more stable (around 0.6) and became less variable. The r_s values were higher at the end of the season and tended to increase after each pruning. The selected Sentinel-2 NDVI maps are shown in Fig. 7 with a red asterisk and correspond to DOY 221, 211, 165 and 195 from 2019 to 2022, respectively. These images were the first to have $Tr_s = 0.60$ in the season, and so are considered to present similar spatial patterns to those of the LLI map prior to harvest.

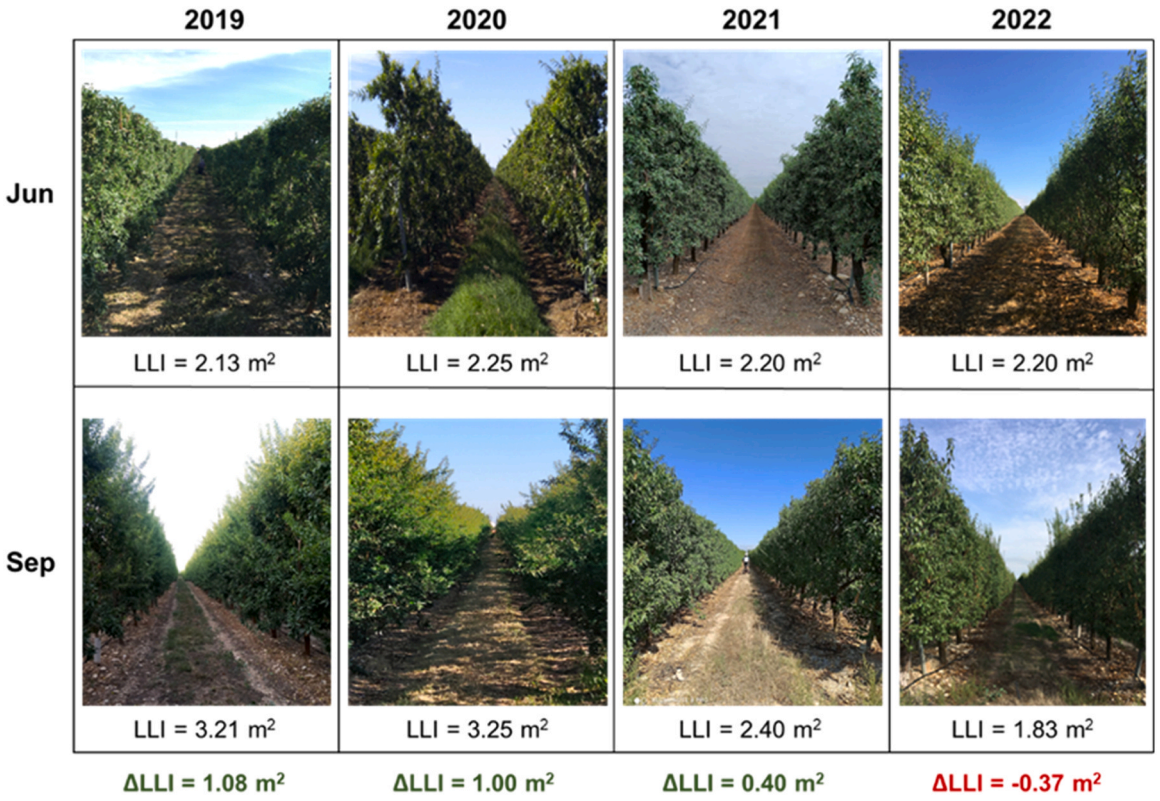

Fig. 5. Photos and LLI values in the super-intensive almond orchard during the study years estimated in June (after pruning) and in September (before harvesting).

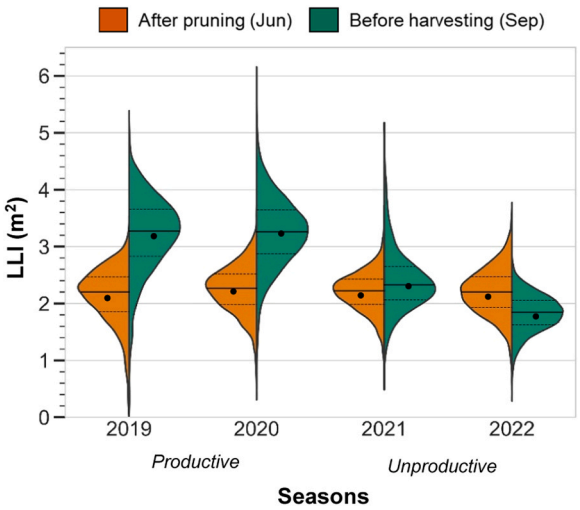

Fig. 6. Leafiness LiDAR index (LLI) intra- and inter-annual variability observed across the analysed years. Left halves of the violin plots represent values after summer pruning (June) while the right halves represent the values before harvesting (September). The black dots indicate the mean value. The solid horizontal lines indicate the median value. Upper and lower dashed lines indicate the 75th and 25th quantiles, respectively.

These images correspond to 54 and 55 days (about two months) after summer pruning for the productive seasons (2019 and 2020, respectively) and up to two weeks for the unproductive seasons (2021 and 2022, respectively). 2019 presented the highest number of pruning interventions and had the highest variability after summer pruning. It was observed that when NDVI increased, the r_s tended to decrease.

Weeding was carried out before summer pruning to facilitate subsequent management. In the case of 2019, it was not possible to discern the effect of pruning compared to weeding as both were carried out almost simultaneously. However, for the other years this effect could be seen both in the decrease of the NDVI values and in the increase of r_s.

3.3. Model-based clustering approach to delineate potential management zones (PMZs)

After applying the model-based clustering (*mclust*), three models were found to be the best performing models. All of them indicated that two PMZs were optimal (Fig. 8, left). However, the model with the best performance was the EEV model (higher BIC: −881.03). After the application of the *clustvarsel* algorithm, all variables, including Sentinel-2 NDVI maps and shallow and deep ECa, were included as significant. This model was built with the six variables that are shown in Fig. 8 (top). In the ECa maps, the soil texture map was also presented. Of the total variability, 60.2 % was explained by the EEV model, determining that the delimited clusters had an ellipsoidal distribution, equal volume and equal shape. The two clusters that defined the PMZs had an equal number of pixels (n= 27). The PMZ spatial distribution is shown in Fig. 8 (right). The model PMZ delineation was validated using post hoc ANOVA tests with the LLI values obtained at the end of each season (Table 3). The EEV model found a consistent PMZ delineation that was significant for all years, regardless of whether the year was productive or unproductive. Furthermore, this PMZ delineation corresponded to significant differences in LLI values (Table 3). Cluster 1, associated with clay loam, exhibited the highest LLI, NDVI, and shallow ECa values, while Cluster 2, linked with silt loam, showed higher deep ECa values.

4. Discussion

The response of almond trees to different management practices has been analysed in the scientific literature by different authors using physiological and morphological determinations to estimate, among other parameters, the water status of trees and their vegetative growth

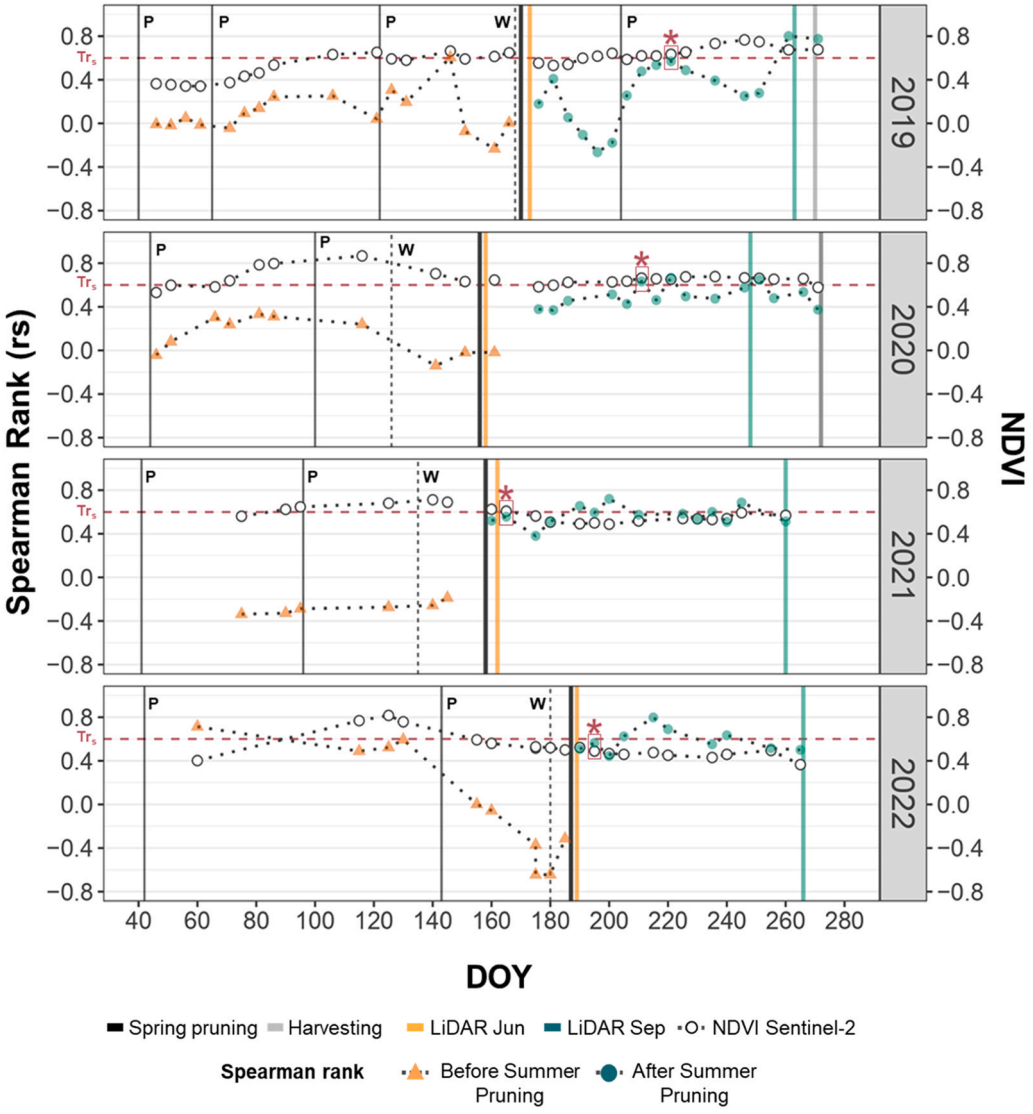

Fig. 7. Evolution of Spearman's rank correlation between LLI measured a few days before harvest and NDVI measured during the mid-season period over the four considered years (2019, 2020, 2021 and 2022). Letters P and W in the graph correspond to pruning and weeding, respectively. $Tr_s = 0.60$ is represented by the dashed red line. The selected Sentinel-2 images are indicated with a red asterisk. DOY is the continuous count of days from the 1st of January.

(Egea et al., 2013; Bellvert et al., 2021). The present study aims to take a further step in the management of super-intensive orchards by assessing the effects of agronomic practices on orchard dynamics and by determining the best moment in the growing season to delineate stable PMZs. To this end, a multitemporal decision-making approach using remote and proximal sensing was applied in a super-intensive almond orchard.

In this research, the LLI, developed by Sandonis-Pozo et al. (2023), was computed at critical stages in orchard management: immediately after summer pruning and just before harvest across four consecutive growing seasons (2019–2022). Figs. 5 and 6 show that LLI values, and therefore, canopy LAI varied significantly between productive and unproductive years. More specifically, LLI values were higher and more variable in 2019 and 2020 compared to 2021 and 2022. These variations in LAI estimates can be attributed to different management practices shown in Tables 1 and 2. In response to commercial considerations and frost-related yield losses, reduced fertigation rates were implemented in the latter two seasons, particularly notable in 2022. This reduction in water and nutrient application led to stress conditions and increased leaf drop, resulting in lower LAI estimates observed in September 2022 compared to June 2022, as shown in Fig. 5.

The results of the study show that, except for 2022, LLI values were higher and more variable towards the end of the season. This trend was expected as early season LLI measurements were consistently taken immediately after summer pruning and inter-row weed removal. However, variations in mean, median, and quantile values of LLI observed in June suggest inconsistencies in pruning practices. These variations could be due to differences in pruning intensity or timing which affect the geometric and structural parameters of the orchard hedgerows and subsequently LAI estimation. Such variability in pruning practices affecting orchard management outcomes is a well-documented issue. For example, Martín-Gorriz et al. (2021) studied lemon orchards and highlighted the challenges of quantifying wood removal in mechanical pruning. Similarly, Jiménez-Brenes et al. (2017) used UAV technology and advanced object-based image analysis (OBIA) to monitor olive trees and found that pruning type and severity significantly influenced leaf drop and annual canopy growth patterns.

The study at hand also presents a methodology based on Sentinel-2 NDVI time series to improve orchard management. This methodology was applied to find an optimal NDVI date(s) that could be used as a reference for possible pre-harvest crop treatments, such as N treatments, precision pruning and/or spraying. It can be concluded from Fig. 7 that the NDVI presented low intra-season variability. These findings agree

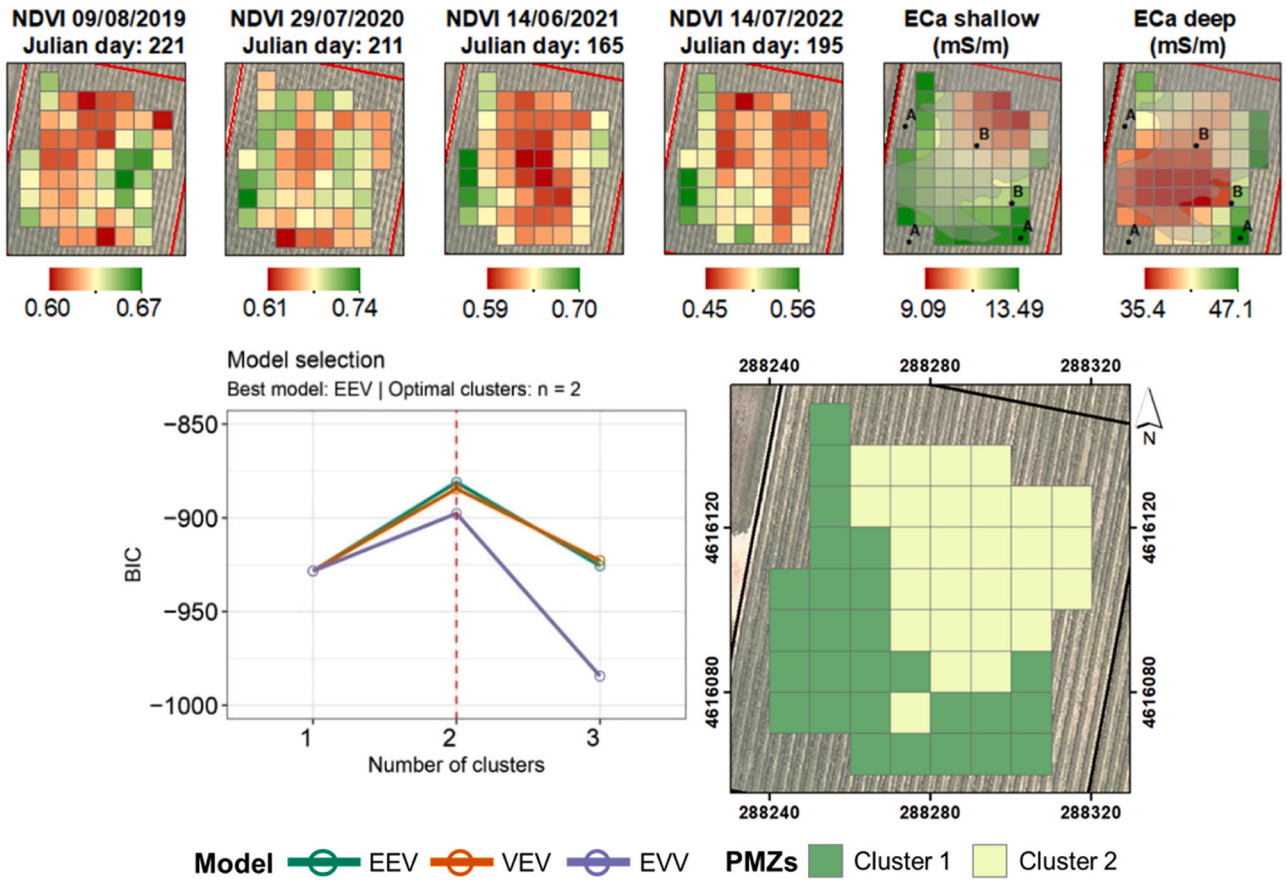

Fig. 8. Variable selection for the model. In the ECa maps, A and B correspond to clay loam and silt loam, respectively (top). mclust best models and optimal clusters (left). Spatial distribution of PMZs (right): Clusters 1 and 2. EEV: ellipsoidal, equal volume and equal shape; VEV: ellipsoidal, equal shape; EVV: ellipsoidal, equal volume. Projection and zone and datum (UTM 31 T/ETRS89).

Table 3
LLI values per zone and Student's t-test for the EEV model.

PMZ	LLI 2019	LLI 2020	LLI 2021	LLI 2022
1	3.39	3.38	2.39	1.92
2	3.23	3.26	2.29	1.77
p-value	0.0013	0.0028	0.0051	0.0001

with the results published by Morell-Monzó et al. (2023), who established that perennial crops have low spectral variation during the year. Fig. 7 shows that, comparing the NDVI behaviour during the four years irrespective of whether the season was productive or unproductive, some orchard dynamics were similar, especially after and before summer pruning.

Before weeding and summer pruning, NDVI values typically peaked during the season, particularly around April-May. During this period, Spearman's rank correlations (r_s) showed greater variability and lower correlations between Sentinel-2 NDVI and end-of-season LLI maps. This variability can be attributed to higher vegetation growth rates in spring and the presence of inter-row weeds. Fig. 5 shows that the presence of inter-row weeds was significantly higher in 2020, coinciding with the year of highest recorded rainfall (Table 2), suggesting that the presence of weeds may have influenced the increased NDVI values. This may compromise the potential effective use of remote sensing imagery in almond orchards. These findings are consistent with the recommendations of Arquero and Jarvis-Shean. (2017), who considered that having associated crops (or 'inter-crops') between tree rows, such as annual herbaceous crops, is not recommendable as they could delay the onset of production and complicate orchard management. Therefore, this study recommends that almond remote sensing should be carried out after row weeding removal is completed in order to mitigate these problems.

After summer pruning, the NDVI became more homogeneous. The r_s values were also higher and more stable in all seasons, reaching the Tr_s (0.60) about two months after summer pruning in productive years but only two weeks after summer pruning in unproductive years. The greater stability of the Spearman coefficient after summer pruning may be due to two factors. Firstly, weeding took place just before summer pruning, making the NDVI more homogeneous, and secondly, as a consequence of N competition between the functional pool of N allocated to vegetation development and that allocated to fruiting (Zarate-Valdez et al., 2015). Fig. 7 shows that a single image per season could be sufficient to indicate the canopy characteristics of an orchard until harvest and the resulting spatial patterns. However, this study highlights the importance of knowing the date of the beginning of the stabilization of r_s values, as the timing differed when comparing productive and unproductive seasons.

Although almonds are a perennial crop typically associated with stability over time (Kazmierski et al., 2011), this study revealed significant inter-seasonal variability (Fig. 7). This variability can be attributed to several factors, including inherent factors such as soil and weather conditions as well as human-induced factors such as management practices. Previous research, such as that by Tombesi et al. (2011), has shown that critical processes in almond growth, such as flowering, fruit set and yield, are influenced by annual variations in canopy management and environmental conditions. In the first productive season (2019), canopy vegetation imbalances and natural growth were higher, leading to increased pruning interventions. However, despite more frequent pruning, it did not result in the highest production. These

findings are in line with those of Dias et al. (2022), who suggested that the intensity and frequency of pruning interventions could have a negative impact on yield if not appropriately spaced.

Another question that this study sought to assess was whether, despite the inter-seasonal variability, there were some PMZs with stable patterns over time. Although cluster analysis is the most commonly used and recommended method for cluster delineation in precision agriculture (Taylor et al., 2007; Martínez-Casasnovas et al., 2018), to the best of the authors' knowledge, there is still no accepted protocol or guidelines for establishing PMZs in orchards, and different methodologies are available. Most of the studies found in the scientific literature have established management zones by considering a single image or a time series (Rivera et al., 2022). The accumulated NDVI has also been shown to be a good predictor of yield in orchards (Martínez-Casasnovas et al., 2018). However, in light of the results obtained in this research, there are several factors involved in orchard variability, such as soil characteristics or canopy management, which should be considered when delineating PMZs.

The *mclust* algorithm used in this study has been recognized for its ability to handle high-density data files with multiple variables (Scrucca et al., 2023). Furthermore, it removes uncertainty in the determination of PMZ delineation, which is often subjective in precision agriculture, by providing a robust method for grouping data within a statistical modelling framework. This algorithm improves PMZ determination by providing an objective approach to spatially organising orchard variability through data-driven clustering techniques. Recent studies have demonstrated the utility of this algorithm for clustering spatio-temporal data (Cheam et al., 2017; Mouret et al., 2021). In this study, the EEV model found a consistent PMZ delineation that was significant for all years, regardless of whether the year was productive or unproductive (Table 3). Furthermore, this PMZ delineation corresponded to significant differences in LLI values. Our findings are in line with those of Georgi et al. (2018), who used NDVI satellite data to delineate cropping patterns as relative yield expectation zones, emphasizing the influence of previous cropping conditions.

Regarding the relationship between PMZs and soil properties, Cluster 1 was associated with clay loam. This zone showed higher vegetative vigour and shallow ECa values, whereas Cluster 2, associated with silt loam, showed higher deep ECa values. These results are consistent with previous studies. Hubbard et al. (2021) observed a similar relationship between higher soil clay content and higher NDVI values in vineyards. The authors linked the benefits of finer textured soils to increased water retention capacity, resulting in increased vegetative vigour. Uribeetxebarria et al. (2018) conducted a study in an area similar to that of the present study, characterised by the presence of a petrocalcic horizon at variable depths. They found that the abundant presence of carbonate content in the subsoil had a clear effect on increasing ECa at depth.

5. Conclusions

This paper presents a method that provides valuable decision-support information for orchard management based on orchard dynamics and stable temporal patterns from previous seasons.

Variability in LAI estimates across seasons was attributed to different management decisions, such as varying fertigation inputs and pruning practices. Orchard dynamics were notably influenced by the intensity and timing of management practices, particularly summer pruning and weeding. After the summer pruning and in the absence of inter-row weeds, NDVI was a good indicator of the spatial organization of LAI. The model-based clustering approach proved effective in delineating potential management zones (PMZs), that remained consistent across productive and unproductive seasons. These PMZs correlated with significant differences in LAI estimates, suggesting their utility as a framework for implementing effective site-specific management practices in future seasons.

This methodology can potentially be adapted for use in other orchards with similar training systems and 3D architecture, such as super-intensive olive trees, extending its applicability to various perennial crops.

CRediT authorship contribution statement

L. Sandonís-Pozo: Writing – original draft, Investigation, Formal analysis, Data curation. **B. Oger:** Writing – review & editing, Methodology, Formal analysis, Data curation. **B. Tisseyre:** Writing – review & editing, Supervision, Methodology, Conceptualization. **J. Llorens:** Writing – review & editing, Software, Methodology, Investigation, Data curation. **A. Escolà:** Writing – review & editing, Methodology, Data curation, Conceptualization. **M. Pascual:** Writing – review & editing, Supervision, Methodology, Conceptualization. **J.A. Martínez-Casasnovas:** Writing – review & editing, Supervision, Project administration, Conceptualization.

Declaration of Competing Interest

The authors declare that they have no known competing financial interests or personal relationships that could have appeared to influence the work reported in this paper.

Data Availability

Data will be made available on request.

Acknowledgments

This research was funded by Grant RTI2018–094222-B-I00 (PAgFRUIT project) and PID2021–126648OB-I00 (PAgPROTECT project) by MCIN/AEI/10.13039/501100011033 and by "ERDF, a way of making Europe" of the European Union. The authors wish to thank Alrasa Agraria S.L. (Raimat, Lleida), the Centre for Technological and Industrial Development (Ministry of Science and Innovation, Government of Spain) and EuroChem Iberia S.A. for providing funds and experimental facilities, and to the members of the Research Group in AgroICT and Precision Agriculture (GRAP) of the Universitat de Lleida for their collaboration in data acquisition.

References

Arquero, O., Jarvis-Shean, K., 2017. Orchard Management, in: Socias i Company, R., Gradziel, T.M. (Eds.), Almonds, Botany, Production and Uses. CAB International, Boston, MA, pp. 240-253.

Barajas, E., Álvarez, S., Fernández, E., Vélez, S., Rubio, J.A., Martín, H., 2020. Sentinel-2 satellite imagery for agronomic and quality variability assessment of pistachio (Pistacia vera L.). Sustainability 12 (20), 8437. https://doi.org/10.3390/SU12208437.

Bellvert, J., Nieto, H., Pelechá, A., Jofre-Čekalović, C., Zazurca, L., Miarnau, X., 2021. Remote sensing energy balance model for the assessment of crop evapotranspiration and water status in an almond rootstock collection. Front. Plant Sci. 12, 608967 https://doi.org/10.3389/FPLS.2021.608967/BIBTEX.

Calera, A., Campos, I., Osann, A., D'Urso, G., Menenti, M., 2017. Remote sensing for crop water management: from ET modelling to services for the end users. Sensors 17 (5), 1104. https://doi.org/10.3390/S17051104.

Caruso, G., Zarco-Tejada, P.J., González-Dugo, V., Moriondo, M., Tozzini, L., Palai, G., Rallo, G., Hornero, A., Primicerio, J., Gucci, R., 2019. High-resolution imagery acquired from an unmanned platform to estimate biophysical and geometrical parameters of olive trees under different irrigation regimes. PLoS ONE 14 (1), 1–19. https://doi.org/10.1371/journal.pone.0210804.

Casanova-Gascón, J., Figueras-Panillo, M., Iglesias-Castellarnau, I., Martín-Ramos, P., 2019. Comparison of SHD and open-center training systems in almond tree orchards cv. 'Soleta. Agronomy 9 (12), 1–15. https://doi.org/10.3390/agronomy9120874.

Cheam, A.S.M., Marbac, M., McNicholas, P., 2017. Model-based clustering for spatiotemporal data on air quality monitoring. Environmetrics 28 (3), 1–11. https://doi.org/10.1002/env.2437.

Dias, A., Falcão, J., Pinheiro, A., Peça, J., 2022. Effect of mechanical pruning on olive yield in a high-density olive orchard: an account of 14 years. Agronomy 12 (5), 1–11. https://doi.org/10.3390/agronomy12051105.

Egea, G., Nortes, P.A., Domingo, R., Baille, A., Pérez-Pastor, A., González-Real, M.M., 2013. Almond agronomic response to long-term deficit irrigation applied since

orchard establishment. Irrig. Sci. 31 (3), 445–454. https://doi.org/10.1007/s00271-012-0322-8.
Fang, H., Baret, F., Plummer, S., Schaepman-Strub, G., 2019. An overview of global leaf area index (LAI): methods, products, validation, and applications. Rev. Geophys. 57 (3), 739–799. https://doi.org/10.1029/2018RG000608.
Georgi, C., Spengler, D., Itzerott, S., Kleinschmit, B., 2018. Automatic delineation algorithm for site-specific management zones based on satellite remote sensing data, 19, 684–707. https://doi.org/10.1007/s11119-017-9549-y.
González-Gómez, L., Intrigliolo, D.S., Rubio-Asensio, J.S., Buesa, I., Ramírez-Cuesta, J. M., 2022. Assessing almond response to irrigation and soil management practices using vegetation indexes time-series and plant water status measurements. Agric., Ecosyst. Environ. 339, 108124 https://doi.org/10.1016/j.agee.2022.108124.
Gu, C., Zhai, C., Wang, X., Wang, S., 2021. CMPC: an innovative lidar-based method to estimate tree canopy meshing-profile volumes for orchard target-oriented spray. Sensors 21 (12), 4252. https://doi.org/10.3390/S21124252.
Gu, C., Zhao, C., Zou, W., Yang, S., Dou, H., Zhai, C., 2022. Innovative leaf area detection models for orchard tree thick canopy based on LiDAR point cloud data. Agriculture 12 (8). https://doi.org/10.3390/agriculture12081241.
Guan, H., Huang, J., Li, L., Li, X., Miao, S., Su, W., Ma, Y., Niu, Q., Huang, H., 2023. Improved Gaussian mixture model to map the flooded crops of VV and VH polarization data. Remote Sens. Environ. 295 (6)) https://doi.org/10.1016/j.rse.2023.113714.
Hubbard, S.S., Schmutz, M., Balde, A., Falco, N., Peruzzo, L., Dafflon, B., Léger, E., Wu, Y., 2021. Estimation of soil classes and their relationship to grapevine vigour in a Bordeaux vineyard: advancing the practical joint use of electromagnetic induction (EMI) and NDVI datasets for precision viticulture. Precis. Agric. 22 (4), 1353–1376. https://doi.org/10.1007/s11119-021-09788-w.
Jiménez-Brenes, F.M., López-Granados, F., de Castro, A.I., Torres-Sánchez, J., Serrano, N., Peña, J.M., 2017. Quantifying pruning impacts on olive tree architecture and annual canopy growth by using UAV-based 3D modelling. Plant Methods 13 (1), 1–15. https://doi.org/10.1186/S13007-017-0205-3.
Jiwei, X., Bermeo, N., Zheng, M., Langton, D., O'Grady, M., O'Hare, G., 2021. Automated zone identification for variable-rate services in precision agriculture. IEEE Access 9, 163242–163252. https://doi.org/10.1109/ACCESS.2021.3134488.
Johansen, K., Raharjo, T., McCabe, M.F., 2018. Using multi-spectral UAV imagery to extract tree crop structural properties and assess pruning effects. Remote Sens. 10 (6), 854. https://doi.org/10.3390/rs10060854.
Johnson, L.F., Roczen, D.E., Youkhana, S.K., Nemani, R.R., Bosch, D.F., 2003. Mapping vineyard leaf area with multispectral satellite imagery. Comput. Electron. Agric. 38 (1), 33–44. https://doi.org/10.1016/S0168-1699(02)00106-0.
Kasimati, A., Espejo-Garcia, B., Vali, E., Malounas, I., Fountas, S., 2021. Investigating a selection of methods for the prediction of total soluble solids among wine grape quality characteristics using normalized difference vegetation index data from proximal and remote sensing. Front. Plant Sci. 12, 1–10. https://doi.org/10.3389/fpls.2021.683078.
Kazmierski, M., Glémas, P., Rousseau, J., Tisseyre, b, 2011. Temporal stability of within-field patterns of NDVI in non-irrigated Mediterranean vineyards. J. Int. Des. Sci. De. la Vigne Et. du Vin. 45 (2), 61–73. https://doi.org/10.20870/oeno-one.2011.45.2.1488.
Lagrange, A., Fauvel, M., Grizonnet, M., 2017. Large-scale feature selection with gaussian mixture models for the classification of high dimensional remote sensing images. IEEE Trans. Comput. Imaging 3 (2), 230–242. https://doi.org/10.1109/tci.2017.2666551.
Lim, K., Pan, K., Yu, Z., Xiao, R., 2020. Pattern recognition based on machine learning identifies oil adulteration and edible oil mixtures. Nat. Commun. 11 (1) https://doi.org/10.1038/s41467-020-19137-6.
Llorens, J., Cabrera, C., Escolà, A., Arnó, J.R., 2019. Software code to process and extract information from 3D lidar point clouds. In: Stafford, J.V. (Ed.), Poster Proceedings of the 12th European Conference on Precision Agriculture, pp. 114–115.
Mahmud, S., Zahid, A., He, L., Choi, D., Krawczyk, G., Zhu, H., Heinemann, P., 2021. Development of a LiDAR-guided section-based tree canopy density measurement system for precision spray applications. Comput. Electron. Agric. 182, 106053 https://doi.org/10.1016/j.compag.2021.106053.
Maldera, F., Vivaldi, G.A., Iglesias-Castellarnau, I., Camposeo, S., 2021. Two almond cultivars trained in a super-high-density orchard show different growth, yield efficiencies and damages by mechanical harvesting. Agronomy 11 (7), 1406. https://doi.org/10.3390/agronomy11071406.
Martínez-Casasnovas, J.A., Escolà, A., Arnó, J., 2018. Use of farmer knowledge in the delineation of potential management zones in precision agriculture: a case study in maize (Zea mays L.). Agriculture 8 (6), 84. https://doi.org/10.3390/agriculture8060084.
Martín-Gorriz, B., Martinez-Barba, C., Torregrosa, A., 2021. Lemon trees response to different long-term mechanical and manual pruning practices. Sci. Hortic. 275, 1–8. https://doi.org/10.1016/j.scienta.2020.109700.
Mirás-Avalos, J.M., Gonzalez-Dugo, V., García-Tejero, I.F., López-Urrea, R., Intrigliolo, D.S., Egea, G., 2023. Quantitative analysis of almond yield response to irrigation regimes in Mediterranean Spain. Agric. Water Manag. 279, 108208 https://doi.org/10.1016/j.agwat.2023.108208.
Moon, K.W., 2016. Violin Plot, in: Learn ggplot2 Using Shiny App. Use R!, first edition. Springer, Cham. pp-191-200.
Morell-Monzó, S., Sebastiá-Frasquet, M.T., Estornell, J., Moltó, E., 2023. Detecting abandoned citrus crops using Sentinel-2 time series. a case study in the comunitat valenciana region (Spain). ISPRS J. Photogramm. Remote Sens. 201, 54–66. https://doi.org/10.1016/j.isprsjprs.2023.05.003.
Mouret, F., Albughdadi, M., Duthoit, S., Kouam'e, D., Rieu, G., Tourneret, J., 2021. Reconstruction of Sentinel-2 derived time series using robust Gaussian mixture models – Application to the detection of anomalous crop development. Comput. Electron. Agric. 198, 106983 https://doi.org/10.1016/j.compag.2022.106983.
Ouazaa, S., Jaramillo-Barrios, C., Chaali, N., Amaya, Y., Carvajal, J., Ramos, O., 2022. Towards site specific management zones delineation in rotational cropping system: application of multivariate spatial clustering model based on soil properties. Geoderma Reg. 30 (2), e00564 https://doi.org/10.1016/j.geodrs.2022.e00564.
Pokovai, K., Fodor, N., 2019. Adjusting ceptometer data to improve leaf area index measurements. Agronomy 9 (12), 866. https://doi.org/10.3390/agronomy9120866.
Ratcliff, C., Gobbett, D., Bramley, R., 2020. PAT - Precision Agriculture Tools Plugin v1.0.4. (Version 1.0.4). QGIS. ⟨https://plugins.qgis.org/plugins/pat/version/1.0.4/⟩.
Rivera, A.J., Pérez-Godoy, M.D., Elizondo, D., Deka, L., del Jesus, M.J., 2022. Analysis of clustering methods for crop type mapping using satellite imagery. Neurocomputing 492, 91–106. https://doi.org/10.1016/j.neucom.2022.04.002.
Rodríguez, A., Benítez Piccini, E., Muñoz, A., 2018. Tolerancia a las heladas por superenfriamiento en cultivares de nogal (Juglans regia) y almendro (Prunus amygdalus). RIA: revista de investigación. Agropecuaria 44 (1), 101–110.
Rosenblad, A., 2011. The concise encyclopedia of statistics. J. Appl. Stat. 38 (4), 867–868. https://doi.org/10.1080/02664760903075614.
Saifuzzaman, M., Adamchuk, V., Buelvas, R., Biswas, A., Prasher, S., Rabe, N., Aspinall, D., Ji, W., 2019. Clustering tools for integration of satellite remote sensing imagery and proximal soil sensing data. Remote Sens. 11 (9), 1–17. https://doi.org/10.3390/rs11091036.
Sandonís-Pozo, L., Llorens, J., Escolà, A., Arnó, J., Pascual, M., Martínez-Casasnovas, J. A., 2022. Satellite multispectral indices to estimate canopy parameters and within-field management zones in super-intensive almond orchards. Precis. Agric. 23, 2040–2062. https://doi.org/10.1007/s11119-022-09956-6.
Sandonís-Pozo, L., Martínez-Casasnovas, J.A., Escolà, A., Rosell-Polo, J.R., Rufat, J., Pascual, M., 2023. A new leafiness-LiDAR index to estimate light interception in intensive olive orchards. In: Stafford, J.V. (Ed.), Proceedings of the 14th European Conference on Precision Agriculture, pp. 189–195. https://doi.org/10.3920/978-90-8686-947-3_22.
Scrucca L., Fraley C., Murphy T.B., Raftery A.E., (2023). Model-Based Clustering, Classification, and Density Estimation Using mclust in R, first edition. Chapman and Hall/CRC. doi:10.1201/9781003277965.
Serrano, J., Shahidian, S., Marques da Silva, J., Paixão, L., Moral, F., Carmona-Cabezas, R., Garcia, S., Palha, J., Noéme, J., 2020. Mapping Management Zones Based on Soil Apparent Electrical Conductivity and Remote Sensing for Implementation of Variable Rate Irrigation—Case Study of Corn under a Center Pivot. Water 12, 3427. https://doi.org/10.3390/w12123427.
Serrano-Notivoli, R., Lemus-Canovas, M., Barrao, S., Sarricolea, P., Meseguer-Ruiz, O., Tejedor, E., 2022. Heat and cold waves in mainland Spain: origins, characteristics, and trends. Weather Clim. Extrem. 37, 100471 https://doi.org/10.1016/j.wace.2022.100471.
Skakun, S., Wevers, J., Brockmann, C., Doxani, G., Aleksandrov, M., Batič, M., Frantz, D., Gascon, F., Gómez-Chova, L., Hagolle, O., López-Puigdollers, D., Louis, J., Lubej, M., Mateo-García, G., Osman, J., Peressutti, D., Pflug, B., Puc, J., Richter, R., Žust, L., 2022. Cloud mask intercomparison eXercise (CMIX): an evaluation of cloud masking algorithms for Landsat 8 and Sentinel-2. Remote Sens. Environ. 274, 112990 https://doi.org/10.1016/j.rse.2022.112990.
Soil Survey Staff, 2014. Kellogg Soil Survey Laboratory Methods Manual. Soil Survey Investigations Report No. 42, Version 5.0. R. Burt and Soil Survey Staff (Ed.). USDA &NRCS.
Sun, L., Gao, F., Anderson, M.C., Kustas, W.P., Alsina, M.M., Sanchez, L., Sams, B., McKee, L., Dulaney, W., White, W.A., Alfieri, J.G., Prueger, J.H., Melton, F., Post, K., 2017. Daily mapping of 30 m LAI and NDVI for grape yield prediction in California vineyards. Remote Sens. 9 (4), 317. https://doi.org/10.3390/rs9040317.
Taylor, J.A., McBratney, A.B., Whelan, B.M., 2007. Establishing management classes for broadacre agricultural production. Agron. J. 99 (5), 1366–1376. https://doi.org/10.2134/AGRONJ2007.0070.
Tombesi, S., Lampinen, B.D., Metcalf, S., Dejong, T.M., 2011. Relationships between spur-and orchard-level fruit bearing in almond (Prunus dulcis). Tree Physiol. 31 (12), 1413–1421. https://doi.org/10.1093/treephys/tpr119.
Torres-Sánchez, J., de Castro, A.I., Peña, J.M., Jiménez-Brenes, F.M., Arquero, O., Lovera, M., López-Granados, F., 2018. Mapping the 3D structure of almond trees using UAV acquired photogrammetric point clouds and object-based image analysis. Biosyst. Eng. 176, 172–184. https://doi.org/10.1016/j.biosystemseng.2018.10.018.
Uribeetxebarria, A., Arnó, J., Escolà, A., Martínez-Casasnovas, J.A., 2018. Apparent electrical conductivity and multivariate analysis of soil properties to assess soil constraints in orchards affected by previous parcelling. Geoderma 319, 185–193. https://doi.org/10.1016/j.geoderma.2018.01.008.
Vélez, S., Rançon, F., Barajas, E., Brunel, G., Rubio, J.A., Tisseyre, B., 2022. Potential of functional analysis applied to Sentinel-2 time-series to assess relevant agronomic parameters at the within-field level in viticulture. Comput. Electron. Agric. 194, 106726 https://doi.org/10.1016/J.COMPAG.2022.106726.
Waskom, M., 2021. Seaborn: Statistical Data Visualization. J. Open Source Softw. 6 (60), 3021. https://doi.org/10.21105/joss.03021.
Westling, F., Underwood, J., Bryson, M., 2021. A procedure for automated tree pruning suggestion using LiDAR scans of fruit trees. Comput. Electron. Agric. 187, 106274 https://doi.org/10.1016/J.COMPAG.2021.106274.
Zarate-Valdez, J.L., Whiting, M.L., Lampinen, B.D., Metcalf, S., Ustin, S.L., Brown, P.H., 2012. Prediction of leaf area index in almonds by vegetation indexes. Comput. Electron. Agric. 85, 24–32. https://doi.org/10.1016/j.compag.2012.03.009.

Zarate-Valdez, J.L., Muhammad, S., Saa, S., Lampinen, B.D., Brown, P.H., 2015. Light interception, leaf nitrogen and yield prediction in almonds: a case study. Eur. J. Agron. 66, 1–7. https://doi.org/10.1016/J.EJA.2015.02.004.

Zhang, C., Yang, G., Jiang, Y., Xu, B., Li, X., Zhu, Y., Lei, L., Chen, R., Dong, Z., Yang, H., 2020. Apple tree branch information extraction from terrestrial laser scanning and backpack-LiDAR. Remote Sens. 12 (21), 1–17. https://doi.org/10.3390/rs12213592.

Zude-Sasse, M., Akbari, E., Tsoulias, N., Psiroukis, V., Fountas, S., Ehsani, R., 2021. Sensing in Precision Horticulture. In: Kerry, R., Escolà, A. (Eds.), Sensing Approaches for Precision Agriculture. Springer, Cham, Switzerland, pp. 221–251.